

1           **Topographic roughness on forested hillslopes: a**  
2           **theoretical approach for quantifying hillslope sediment**  
3           **flux from tree throw**

4           **Tyler H. Doane<sup>1</sup>, Douglas Edmonds<sup>1</sup>, Brian J. Yanites<sup>1</sup>, Quinn Lewis<sup>2</sup>**

5           <sup>1</sup>Indiana University-Bloomington, Department of Earth and Atmospheric Sciences, Bloomington, IN, USA

6           <sup>2</sup>Waterloo University, Department of Geography and Environmental Management, Waterloo, ON, CA

7           **Key Points:**

- 8           • The expected topographic variance is a function of the ratio of tree throw rates  
9           to creep-like diffusivity.
- 10          • Tree throw accounts for 10-20% of the hillslope sediment flux in southern Indi-  
11          ana.
- 12          • Tree throw occurs more frequently on steep, east facing hillslopes which is con-  
13          sistent with the dominant wind directions.

---

Corresponding author: Tyler Doane, [doanet@iu.edu](mailto:doanet@iu.edu)

**Abstract**

Tree uprooting is an observable and consequential process that suddenly moves soil downslope, inverts the soil column, and roughens the surface with pit-mound topography. Quantifying fluxes due to tree throw is complicated by its stochastic nature and estimation requires averaging over a large area or long time. Here, we develop theory that leads to a dimensionless metric directly measurable from high resolution topographic data. The theory explains the flux and topographic roughness as a function of tree throw production and decay rate by creep-like processes. We then form a dimensionless variable that is the ratio of fluxes due to tree throw versus creep-like processes. Applying the theory to hillslopes in Southern Indiana, we find that tree throw accounts for 10 to 20% of the hillslope sediment flux. The theoretical and observational findings provide a framework and important constraints on quantifying Critical Zone function from topographic parameters such as roughness.

**Plain Language Summary**

When trees fall on hillslopes, they often uproot a volume of soil that is attached to the roots. Because trees usually fall downslope, this uprooted soil also moves down the hillslope, contributes to erosion, and leaves characteristic pit and mound shapes on the surface. Despite the topographic signature of the process, quantifying how much dirt trees move downslope is complicated by the randomness that drives the process. We develop theory that explains the roughness of hillslope topography and how it relates to sediment transport rates driven by tree throw. We then map topographic roughness over a county in southern Indiana and demonstrate that tree throw accounts for 10 to 20% of the sediment motions on hillslopes. Further, we demonstrate that east facing hillslopes tend to have more tree throw events which coincides with the dominant wind directions and illustrates that extreme wind events drive most tree throw events in southern Indiana.

**1 Introduction**

The rate and style of sediment transport processes on hillslopes are central to understanding landscape evolution (Roering et al., 2001, 2007), geochemical cycling (Maher, 2010; Yoo et al., 2007; Lebedeva & Brantley, 2013), soil production (Heimsath et al., 2001; Mudd & Furbish, 2004; Gabet & Mudd, 2010; Riebe et al., 2003; Ferrier & Kirchner, 2008),

45 sediment supply to watersheds (Syvitski, 2003), and the dynamics of the Critical Zone  
46 (Brantley, McDowell, et al., 2017; Brantley, Eissenstat, et al., 2017). On hillslopes, a suite  
47 of processes that include freeze-thaw (Anderson, 2002), wetting-drying (Struck et al., 2018),  
48 and bioturbation (Gabet et al., 2003) disturb unconsolidated soil and sediment which  
49 leads to bulk downslope creep-like motion (Culling, 1963; Furbish et al., 2009). Obser-  
50 vation and quantification of these creep-like processes is often obfuscated by the small  
51 scale over which they operate and the slow bulk transport rates that they produce. Tree  
52 throw, however, is a sediment transport process that occurs when trees topple and up-  
53 root a mass of soil – leaving a clear pit-mound couplet as a topographic signature. In  
54 contrast to the suite of creep-like processes, tree throw suddenly moves and mixes soil,  
55 which inverts any soil-depth varying chemical or physical properties. Tree throw there-  
56 fore is a uniquely consequential and measurable process on hillslopes, yet the relative mag-  
57 nitudes of sediment fluxes due to tree throw and creep-like processes remain unknown.

58 Tree throw has been the subject of many field and numerical studies that quan-  
59 tify the sediment flux, (Gabet et al., 2003; Martin et al., 2013; Phillips et al., 2017; Han-  
60 cock & Lowry, 2021; Šamonil et al., 2020) or demonstrate the consequences for weath-  
61 ering and soil production (Gallaway et al., 2009; Gabet & Mudd, 2010; Šamonil et al.,  
62 2013). Quantifying the sediment flux due to tree throw typically involves measuring the  
63 volumes of sediment attached to uprooted trees and constraining event frequency by ei-  
64 ther dating material deposited beneath mounds (Schaetzl & Follmer, 1990; Šamonil et  
65 al., 2013) or by tree census (Gallaway et al., 2009; Martin et al., 2013; Šamonil et al.,  
66 2020). However, tree throw is often caused by rare extreme wind events that impart a  
67 drag force on the canopy which exceed a resisting force of the soil. Such events occur with  
68 a large range of magnitudes and the recurrence intervals for large events can be on the  
69 order of decades (Gallaway et al., 2009; Hancock & Lowry, 2021). Therefore, quanti-  
70 fication of tree throw by direct human observation is beyond our capabilities and requires  
71 that we average over the full range of the process. This requires either a very long record  
72 through time or very large domain that samples a great number of tree throw events.  
73 The land surface is a faithful record of past tree throw events as it accumulates pit-mound  
74 couplets through time and the topographic roughness of a surface reflects a long record  
75 of tree throw events.

76 In this paper, we develop theory for the expected topographic roughness (quanti-  
77 fied by the topographic variance) of a hillslope for a given frequency of tree throw events

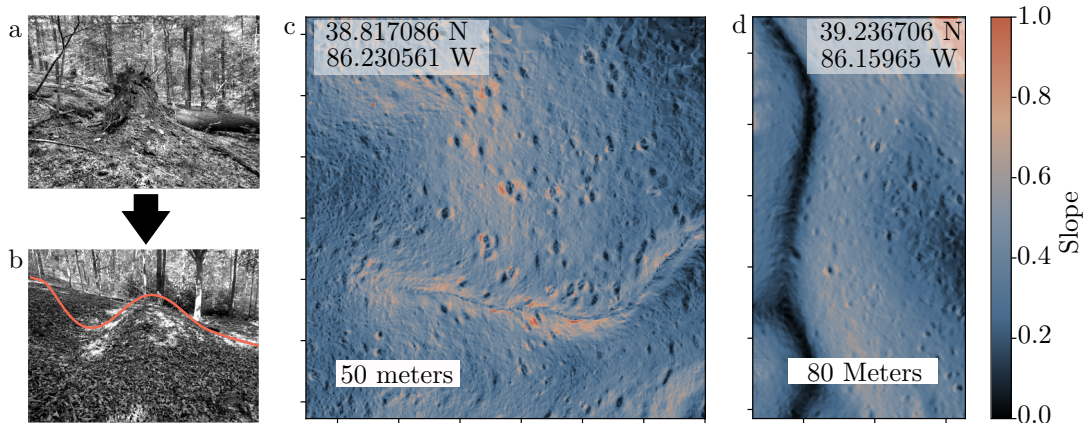


**Figure 1.** (A) Image of a tree throw root ball and (B) the subsequent transition to a characteristic pit-mound couplet. On many hillslopes in southern Indiana pit-mound couplets are the primary roughness features which creates the pocked texture. This texture is visible from (C) 0.25 m and (D) 0.76 m resolution digital elevation models. Hatch marks on the images are equal intervals of meters.

78 and magnitude of topographic smoothing from creep-like processes. We then leverage  
 79 the theory to form a dimensionless variable that is composed entirely of measurable to-  
 80 pographic variables and is the ratio of the hillslope sediment flux due to tree throw ver-  
 81 sus all creep-like processes. Topographic roughness created by tree throw is observable  
 82 in high resolution topographic data and the theory may be applied across large areas.  
 83 We apply the theory to 1,910 hillslopes selected from over 800 km<sup>2</sup> in southern Indiana  
 84 (Brown County) to obtain estimates of the percentage of the flux due to tree throw. We  
 85 demonstrate that tree throw accounts for approximately 10-20% of the hillslope sediment  
 86 flux and highlight an aspect-dependency that is consistent with dominant wind direc-  
 87 tions in southern Indiana.

## 88 2 Theory

89 Here we construct the ratio of sediment flux due to tree throw versus creep-like pro-  
 90 cesses. We develop analytical expressions for the flux due to tree throw and the expected  
 91 topographic variance that reflects the balance between roughness production by tree throw  
 92 and roughness erasure by creep-like processes. These two components are then combined  
 93 to form the desired ratio of volumetric fluxes.

94 **2.1 Flux due to tree throw**

95 Previous work quantifies the flux due to tree throw as the product of the frequency  
 96 of the process and the volume that it mobilizes, which can be measured from the vol-  
 97 umes of either pits or uprooted sediment attached to roots (Gabet et al., 2003; Gallaway  
 98 et al., 2009; Hellmer et al., 2015; Phillips et al., 2017). We present a similar formulation,  
 99 but cast it in probabilistic terms for particle travel distances. The mean flux for any pro-  
 100 cess is (Furbish & Haff, 2010; Doane et al., 2018)

$$\bar{q}(x, y) = E(x, y)\mu_r(x, y) \quad (1)$$

101 where  $E$  [ $L^3 L^{-2}T^{-1}$ ] is a volumetric entrainment rate and  $\mu_r$  is the mean travel dis-  
 102 tance.  $E$  involves the frequency of tree throw events per unit area and the volume of root  
 103 balls, which is a stochastic and noise-driven component that is not directly measurable  
 104 over short timescales or small spatial scales. In contrast, particle travel distances relate  
 105 directly to the geometry of pit-mound couplets (Figure 2).

106 We define an initial couplet geometry that is an approximation to those observed  
 107 in nature (Figure 2),

$$\zeta'(x, y) = \frac{2Ax}{l^2} e^{-\left(\frac{x^2}{l^2} + \frac{y^2}{w^2}\right)}, \quad (2)$$

109 where  $\zeta'$  [L] is the land-surface elevation,  $x$  and  $y$  [L] are horizontal positions,  $A$  [ $L^2$ ] is  
 110 a squared amplitude, and  $l$  and  $w$  are characteristic length scales. Note that (2) is a Gaus-  
 111 sian in the  $y$ -direction and a derivative of a Gaussian in the  $x$ -direction. Previous work  
 112 has suggested alternative forms (two anti-symmetric semi-spheres) for the initial con-  
 113 dition of pit-mound couplets (Gabet et al., 2003; Gabet & Mudd, 2010; Martin et al.,  
 114 2013; Šamonil et al., 2020); however, we prefer this formulation as it approximates nat-  
 115 ural couplet geometries and is mathematically simple to work with. The form of (2) rep-  
 116 represents the initial condition of pit-mound couplets once the tree roots have rotted away  
 117 ( 5-10 years after the tree topples in temperate environments (Schaetzl & Follmer, 1990))  
 118 so that the couplet may evolve by creep-like processes. With this definition of the ini-  
 119 tial condition, the ‘throw’ component involves the tree toppling and the decay of roots  
 120 which drops particles and constructs smooth pit-mound couplets. Based on (1), (2), and  
 121 using the idealized geometry of couplets and allowing for  $A$  and  $l$  to be random variables,  
 122 we find that the average flux due to tree throw on a hillslope is (Appendix A),

$$q_{TT}(x, y) = p(x, y) \frac{\sqrt{2\pi}\mu_A (\mu_l^2 + \sigma_l^2)}{\phi}, \quad (3)$$

123

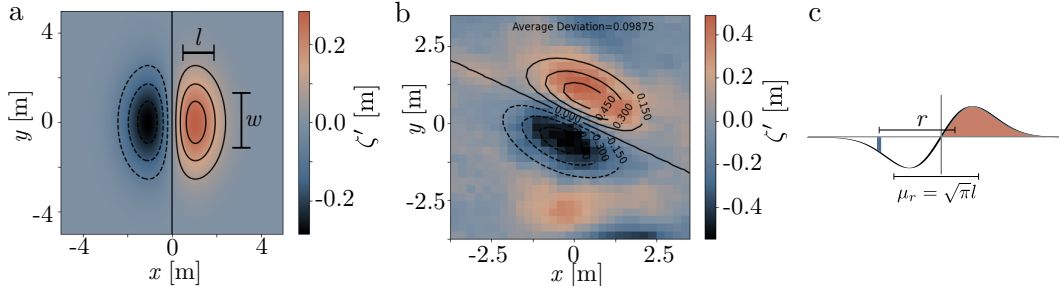


**Figure 2.** (a) Two dimensional view of an idealized pit-mound couplet. (b) Comparison of idealized and natural pit-mound couplet illustrating good agreement. (c) Conceptual diagram illustrating how we calculate the probability function of travel distances,  $r$ .  $l$  and  $w$  are characteristic length scales of pit-mound couplets and  $\mu_r$  is the mean particle travel distance.

124 where  $\mu_X$  and  $\sigma_X^2$  refer to the mean and variance of variable  $X$ , and we have introduced  
 125  $\phi = l/w$  because we expect  $l$  and  $w$  to co-vary on a given slope. The production rate,  
 126  $p$  [ $L^{-2} T^{-1}$ ], is the only variable that is not directly measurable from topography.

127 The idealized pit-mound geometry should vary with slope. When trees fall on pro-  
 128 gressively steeper slopes, more of the uprooted sediment moves further downslope, which  
 129 increases  $l$  and  $\phi$  (Gabet et al., 2003). To account for this we numerically simulate a one-  
 130 dimensional model of pit-mound formation on different slopes which suggests  $l \approx 1 +$   
 131  $S$  where  $S$  is land-surface slope ( $S_4$ ). We note that equation (3) assumes that all trees  
 132 fall directly downslope but, in nature, trees can fall in all directions. However, observa-  
 133 tions of tree throw resulting from ice storms demonstrates that trees typically fall downs-  
 134 lobe (Hellmer et al., 2015), which indicates that they tend to have weaker resiting forces  
 135 in the downslope direction. Most pit-mound couplets are oriented along hillslope con-  
 136 tours in southern Indiana, suggesting that downslope transport is the dominant mode  
 137 of tree throw in this setting.

## 138 2.2 Topographic Roughness

139 Tree throw is the only geomorphic process we know of that adds topographic rough-  
 140 ness to soil mantled and forested hillslopes at the scale of meters. Topographic rough-  
 141 ness can be quantified with the average concavity (Booth et al., 2017; LaHusen et al.,  
 142 2016), fitted polynomial functions (Milodowski et al., 2015), and the standard deviation  
 143 or variance of detrended topography (Roth et al., 2020). We use the topographic vari-

144 ance to quantify roughness because we can derive an analytical solution for the expected  
 145 variance that reflects the balance between tree throw frequency and the pace of couplet  
 146 degradation by creep-like processes.

147 Couplets degrade by the action of all creep-like processes which drive the creation  
 148 and collapse of porosity. When the land-surface is inclined, this leads to downslope sed-  
 149 iment motion at a rate that scales with slope (Furbish et al., 2009). A linear model for  
 150 creep-like processes has a long legacy in geomorphology (Culling, 1963),

$$151 \quad q_c = -D\nabla\zeta, \quad (4)$$

152 where  $q_c$  [ $L^2 T^{-1}$ ] is the volumetric flux,  $D$  [ $L^2 T^{-1}$ ] is a topographic diffusivity, and  $\zeta$   
 153 is the land-surface elevation. Placing (4) into the Exner equation leads to the linear dif-  
 154 fusion equation for the evolution of topography (Fernandes & Dietrich, 1997; Furbish &  
 155 Fagherazzi, 2001; Richardson et al., 2019),

$$156 \quad \frac{\partial\zeta}{\partial t} = D\nabla^2\zeta. \quad (5)$$

157 We note that nonlinear slope- (Roering et al., 2001) and soil thickness-dependent (Furbish  
 158 et al., 2009; Mudd & Furbish, 2004; Johnstone & Hilley, 2015) formulations are alter-  
 159 native flux models. However, neither of these models leads to a significant difference in  
 160 the evolution of topographic variance for pit-mound couplets (S2) so we only consider  
 161 linear diffusion here.

162 We solve the diffusion equation for topography with an initial condition represented  
 163 by (2) to understand the temporal evolution of the topographic variance of a single pit-  
 164 mound couplet. To do so, we transform the problem into the wavenumber domain via  
 165 the Fourier Transform and apply Parseval's Theorem, which states that the integral of  
 166 the square of Fourier Transform amplitudes is equal to the integral of the square of the  
 167 signal in the arithmetic domain (Appendix B). The sum of squares equals the sample  
 168 variance when one divides by the size of the domain so these two steps lead to an an-  
 169 alytical solution for the time evolution of topographic variance of a pit-mound couplet.  
 170 The topographic variance of an entire hillslope is the integral of all couplets of all ages,  
 171 which amounts to a convolution of tree throw production and decay rates,

$$172 \quad \sigma_\zeta^2(t) = \frac{A^2 w^2 l^2 \pi}{32} \int_{-\infty}^t p(t') \left[ \frac{l^2}{4} + D[t-t'] \right]^{-3/2} \left[ \frac{w^2}{4} + D[t-t'] \right]^{-1/2} dt', \quad (6)$$

173 where  $t'$  is an earlier time and  $t-t'$  is a couplet age. Given a time-series of tree throw  
 174 production rates, (6) describes the topographic variance at any moment. The produc-

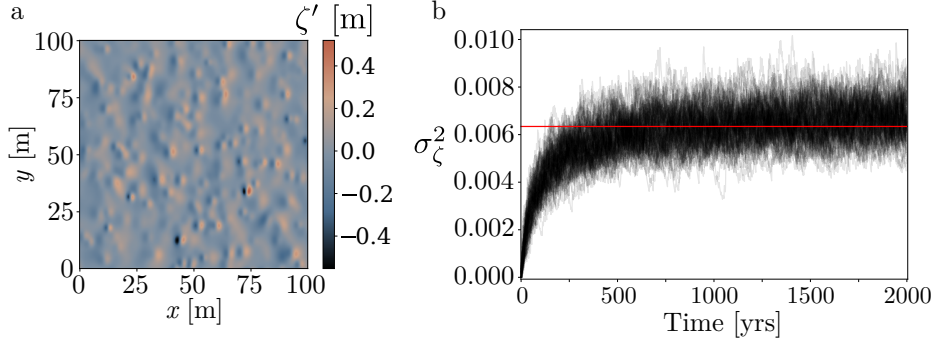


**Figure 3.** a) A rough surface that is the result of a numerical simulation with  $D = 0.005$  and a mean production rate of one tree per year per  $10,000 \text{ m}^2$ . b) The time series of one hundred numerical simulations with the same parameters (gray) and the expected variance (red).

175 tion rate of tree throw will be some noisy signal through time and so too is the time se-  
 176 ries of topographic variance. For the purpose of this paper, we consider the expected to-  
 177 pographic variance, which only involves the mean production rate,  $\mu_p$ . Performing the  
 178 integration in (6) (over all couplets of all ages) yields the expected topographic variance

$$179 \quad E(\sigma_\zeta^2) = \frac{\mu_p A^2 l^2 \pi}{4D(\phi^2 + \phi)}. \quad (7)$$

180 If we allow for  $A$  and  $l$  to be random variables with finite covariance, then the expected  
 181 topographic variance is

$$182 \quad E(\sigma_\zeta^2) = \frac{\mu_p ((\mu_A^2 + \sigma_A^2)(\mu_l^2 + \sigma_l^2) + \text{cov}(A^2, L^2)) \pi}{4D(\phi^2 + \phi)}. \quad (8)$$

183 We numerically test this result by simulating random production and diffusion (equa-  
 184 tion 5) of pit-mound couplets on a flat surface. For each one year time step, a number  
 185 of new pit-mound couplets is selected from an exponential distribution of production rates.  
 186 The exponential distribution reflects our intuition that at a single hillslope and in most  
 187 years, zero to few tree throw events will occur and there will be rare years with many  
 188 tree throw events. The model then populates a two-dimensional domain with new pit-  
 189 mound couplets with parameters that are chosen from distributions that have a small  
 190 but finite amount of covariance. Roughness on the numerical surface initially increases  
 191 until it reaches a steady state value which it oscillates around and coincides with (8) (Fig-  
 192 ure 3).

193 Although (8) accurately predicts the expected topographic variance of the numer-  
 194 ical model, it contains two unknown rate constants,  $\mu_p$  and  $D$ . Previous efforts attempt

195 to understand values of  $D$  from a statistical mechanics (Furbish et al., 2009) or empir-  
 196 ical perspective (Richardson et al., 2019). However, identifying the value of  $D$  for a par-  
 197 ticular landscape remains a challenge and is a source of uncertainty. There are also es-  
 198 timates of tree throw production rates (Schaetzl et al., 1990; Phillips et al., 2017; Šamonil  
 199 et al., 2020), but the stochasticity of tree throw over timescales of decades to centuries  
 200 limits the constraints of  $\mu_p$ .

201 Equation 8 demonstrates that rougher hillslopes reflect a relatively high tree throw  
 202 production rate and low diffusivity. Although we cannot know  $\mu_p$  and  $D$  apriori, we can  
 203 learn about the relative magnitude of the sediment fluxes due to tree throw and creep-  
 204 like processes. First, we rewrite the expression for  $q_{TT}$  by rearranging (8) to solve for  
 205  $\mu_p$ . This places  $\sigma_\zeta^2$  and  $D$  in the numerator of (3). Forming the ratio then leads to,

$$206 \quad R = \frac{q_{TT}}{q_c} = 4\sqrt{2} \frac{\mu_A (\phi + 1) \sigma_\zeta^2}{(\mu_A^2 + \sigma_A^2) |S|}, \quad (9)$$

207 where we have assumed that  $\text{cov}(A^2, L^2)$  is negligible (S3). Note that all parts of (9) are  
 208 measurable from high resolution topographic data. We now turn to calculations of  $R$  by  
 209 measuring  $\sigma_\zeta^2$ ,  $|S|$ , and parameterization of  $A$  and  $\phi$  in a forested landscape.

### 210 **3 Measuring topographic variance and R with high-resolution topog-** 211 **raphy**

#### 212 **3.1 Constraining pit-mound geometry**

213 We parameterize  $A$ ,  $l$ , and  $\phi$  by fitting the idealized couplet geometry to pit-mound  
 214 couplets that are clearly visible in high resolution topography. We fit 101 pit-mound cou-  
 215 plets from 0.25 m resolution, drone-collected lidar (S1). Couplets that we identify from  
 216 lidar are likely to vary in age and therefore may have partially diffused. The shape  $A/(wl)$   
 217 of each pit-mound couplet is a proxy for age, and the youngest will have the largest value  
 218 of this ratio (i.e. tall and narrow). We select the 50 freshest/youngest based on this met-  
 219 ric and extract values for  $\mu_A = 0.68$ ,  $\sigma_A^2 = 0.05$ ,  $\phi = 0.83$ , and  $\text{Cov}(A^2, L^2) = 0.005$   
 220 (S3). The covariance and variance terms are negligible relative to the average values and  
 221 so they may be dropped from (8)

#### 222 **3.2 Measuring Topographic Variance**

223 We used a 2017 lidar survey of Indiana collected via the USGS 3D elevation pro-  
 224 gram, that produced digital elevation models (DEMs) at 0.76 m resolution to measure

225 topographic variance. We emphasize that 0.76 m resolution DEMs are capable of cap-  
226 turing the majority of topographic variance from tree throw (S1). We focus our study  
227 on Brown County, which is a rural county in south-central Indiana with moderate re-  
228 lief (200 meters) and locally steep slopes (up to  $\approx 1$ ). The Borden Group, a Missippian  
229 siltstone interbedded with limestone, underlies the entire county (Thompson & Sowder,  
230 2005). Brown County is south of the southern terminus of the last glacial extent and the  
231 topography lacks glacial roughness features like hummocky topography or glacial errat-  
232 ics so that hillslope roughness is reliably created by tree throw.

233 We manually define 1,910 forested hillslopes in Brown County that are minimally  
234 dissected by first-order gullies. We first run a high-pass filter over 1.5x1.5 km sections  
235 of the land surface with a Gaussian filter with a length scale of 3.8 meters (5 pixels) to  
236 filter out hillslope- and valley-scale topography. The high pass filter highlights a num-  
237 ber of roughness features including pit-mound couplets, channel banks, geologic contacts,  
238 and infrastructure. We manually exclude hillslopes with these other roughness features.  
239 For each area of interest, we calculate the topographic roughness as the variance of the  
240 high pass filter output.

## 241 4 Results

242 Measurements of topographic variance for 1910 hillslopes from Brown county (Fig-  
243 ure 4a) span over an order of magnitude from 0.001 up to 0.03. There is a modest pos-  
244 itive relationship between topographic variance and slope (Figure 4b). However, the spread  
245 of measured variance values also increases with slope. Topographic variance also depends  
246 on slope aspect (Figure 4c) with northeast facing slopes having the largest measured val-  
247 ues and west-facing slopes having the lowest. We observe the same trend in the distri-  
248 bution of average slopes of the hillslopes that we selected with east-facing slopes gen-  
249 erally being steeper than west facing slopes (Figure 4d). The reason for the slope-magnitude  
250 sampling discrepancy between east and west slopes is that there is an aspect-dependent  
251 drainage density in which first order channels and gullies tend to dissect steep west fac-  
252 ing slopes more frequently than steep east facing slopes. This limits our ability to sam-  
253 ple steep west facing slopes as channelization processes overprint the hillslopes.

254 Sediment flux due to tree throw increases by roughly 50% on east facing slopes (Fig-  
255 ure 4f). The average values of  $R$  (calculated by weighting hillslopes by area) vary from

256 0.12 to 0.22 on west- and east-facing slopes respectively (Figure 4e), accounting for  $q_{TT}/(q_c +$   
 257  $q_{TT}) = 11\%$  and  $18\%$  of the hillslope sediment flux on those slopes. Several thousand  
 258 eddy covariance measurements of wind velocity from a nearby AmeriFlux tower demon-  
 259 strate that wind blows most frequently to the northeast and least frequently to the west  
 260 (Novick & Phillips, 2020) suggesting that the larger  $R$  and variance on east-facing hill-  
 261 slopes is caused by wind-blown tree throw as opposed to trees aging or snow loading.

262 The spread in  $R$  values (Figure 4e) should not be interpreted as a range of tree throw  
 263 frequency because it reflects the stochastic nature of tree throw. Only the average value  
 264 of  $R$  is meaningful. By sampling 1910 hillslopes across Brown County, we attempt to ex-  
 265 change space for time so that for each primary direction, we have sampled values that  
 266 approach the full range of natural topographic roughness and the average sample rough-  
 267 ness is approximately equal to the expected roughness for a given population of hillslopes  
 (e.g. east vs west).

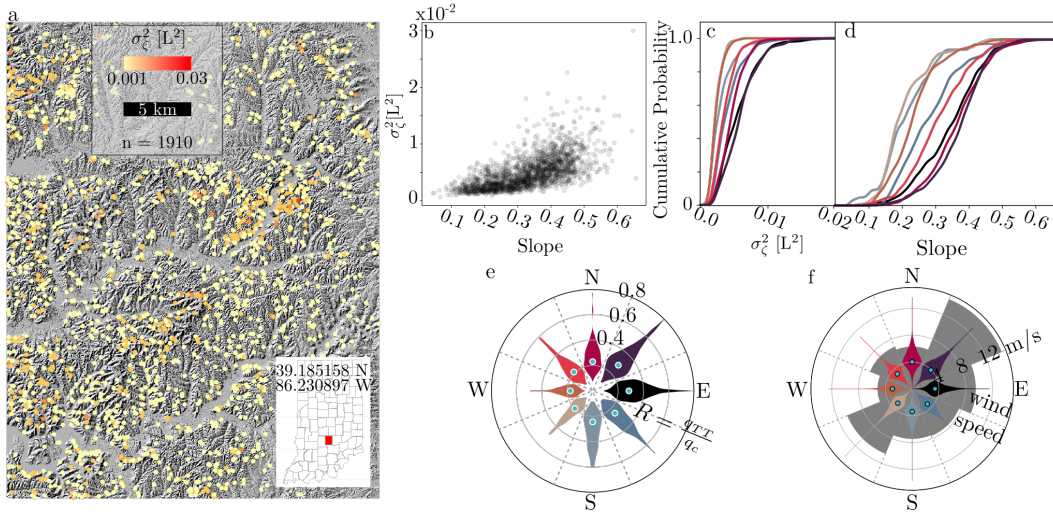


**Figure 4.** a) Hillshade of Brown County, IN with points of selected hillslopes colored by the measured topographic variance. b) Topographic variance as a function of slope. Cumulative probability plots of measured topographic variance (c) and slope (d) colored by aspect. e) Rose diagram of violin plots for  $R$  illustrating a modest aspect dependency. f) Rose diagram of wind speeds (colors) and relative frequencies (gray).

## 5 Discussion and Conclusions

We have developed theory that explains the topographic roughness of forested hillslopes and a tool that maps the relative contributions to the volumetric sediment flux from tree throw and creep-like processes. The topographic variance of a hillslope at any moment is a convolution of a noisy signal through time that depends on the stochastic occurrence of tree throw events and their decay due to creep-like processes. This leads to a noisy signal of topographic roughness that oscillates around an expected value. In general, greater average frequency of tree throw occurrences per area per time and lower values for diffusivity lead to rougher hillslopes (e.g. the  $p/D$  term in Equation 8). This is the first theory to address topographic roughness due to tree throw of forest floors and is key for developing methods for quantifying tree throw.

Our theory assumes that at the scale of meters, pit-mound couplets are the primary roughness feature on hillslopes. Temperate, moderate relief, forested hillslopes lack other sources of roughness such as gopher mounds (Jyotsna & Haff, 1997), sediment mounds that form under shrubs (Worman & Furbish, 2019) (semi-arid), landslides (LaHusen et al., 2016; Booth et al., 2017) and their scarps (steeplands), and solifluction lobes (Glade et al., 2021) (periglacial). Fossorial mammals either produce topographic roughness that are too small (e.g. mole hills) or far too rare (e.g. bear burrows) to explain the observed meter scale roughness in these landscapes. Lithologic contacts in such landscapes are localized and affect few hillslopes. Creep-like processes unconditionally smooth topography (Furbish & Fagherazzi, 2001) so in forested settings we are confident that the topographic roughness in this setting is primarily driven by the production and decay of tree throw couplets.

We have developed a topographic variable,  $R$ , to describe the relative fluxes due to roughening processes (i.e. tree throw) and smoothing processes (e.g. creep).  $R$  is directly measurable from topography and allows for widespread quantification of a process that is driven by stochastic events that occur with frequencies that frustrate direct human observation. The roughness of the land-surface is a record of all past events over timescales of decades to centuries which is required for measuring the contribution to the flux for tree throw. In southern Indiana,  $R$  indicates that tree throw accounts for roughly 11% to 18% of volumetric sediment flux.

300 Despite the clearly rough hillslopes of southern Indiana, 11 to 18% represents a some-  
 301 what modest contribution to the total hillslope sediment flux. However, we suggest that  
 302 tree throw is unlikely to contribute a majority of the volumetric sediment flux for sev-  
 303 eral reasons. First, because soil is an unconsolidated medium, creep will always occur  
 304 (Ferdowsi et al., 2018; Deshpande et al., 2021) and tree throw can never account for all  
 305 of the volumetric flux. Second, although rough hillslopes are common in southern In-  
 306 diana and are clearly observable, there are many more smooth and moderately rough hill-  
 307 slopes (Figure 4b,c,e) that dominate the landscape. Third, tree throw is limited by pop-  
 308 ulation dynamics (Galloway et al., 2009; Gabet & Mudd, 2010) which sets the spacing  
 309 of trees, recruitment of new saplings, and growth rates. All of these may amount to an  
 310 upper limit of  $R$  being around what we have measured in southern Indiana. However,  
 311 further measurement of  $R$  in other settings are required to more definitively quantify the  
 312 limits of tree throw.

313 Despite the relatively small contributions to the volumetric flux, tree throw is a unique  
 314 hillslope transport process that may have an outsized role in influencing Critical Zone  
 315 processes. Tree throw episodically and suddenly creates topographic roughness, inverts  
 316 the soil column, and has the potential to expose fresh bedrock. Each of these has po-  
 317 tential implications to affect hydrologic pathways (Phillips et al., 2017), soil develop-  
 318 ment (Šamonil et al., 2020), chemical weathering, and soil production rates (Gabet &  
 319 Mudd, 2010). We anticipate that  $R$  will be a valuable tool that is readily available for  
 320 quantifying the magnitude and frequency of tree throw and its impact on the Critical  
 321 Zone.

## 322 Appendix A Mean Travel Distance

323 We calculate the mean travel distance by assuming that a particle may be entrained/deposited  
 324 from any location within the pit/mound. The pit and mound individually have a mor-  
 325 phology that resembles a Rayleigh distribution,

$$326 \quad f_z(z) = \frac{2z}{\omega^2} e^{-\frac{z^2}{\omega^2}} \quad (\text{A1})$$

327 where  $z$  is the random variable and  $\omega$  is a parameter. The mean of a Rayleigh distribu-  
 328 tion is

$$329 \quad \mu_r = \frac{\sqrt{\pi}}{2} \omega. \quad (\text{A2})$$

330 The total travel distance is the difference between the mean deposition location and mean  
 331 entrainment location,

$$332 \quad \mu_r(r) = \sqrt{\pi}l. \quad (\text{A3})$$

333 The volumetric entrainment rate, is the volume of the pit multiplied by a production rate,  
 334  $p$  [ $\text{L}^{-2}$ ],

$$335 \quad E(x, y) = p(x, y)\sqrt{\pi}l \int_{-\infty}^{\infty} \int_{-\infty}^0 -\frac{2Ax}{l^2} e^{\left(-\frac{x^2}{l^2} - \frac{y^2}{w^2}\right)} dx dy = p(x, y)\sqrt{2\pi}Awl. \quad (\text{A4})$$

336 Equations (A3) and (A4) combine to form (3).

## 337 Appendix B Topographic Variance

338 The Fourier transform of (1) is

$$339 \quad \hat{\zeta}(k_x, k_y) = -4iAwlk_x\pi e^{-\frac{k_x^2 l^2}{4} - \frac{k_y^2 w^2}{4}}, \quad (\text{B1})$$

340 where  $k_x$  and  $k_y$  is the wavenumber [ $\text{L}^{-1}$ ] (radians per unit length) in the  $x$  and  $y$  di-  
 341 rections. The analytical solution for the diffusion of a couplet through time in wavenum-  
 342 ber domain (B1) is

$$343 \quad \hat{\zeta}(k_x, k_y, t) = -4iAwlk_x\pi e^{-k_x^2(Dt + \frac{l^2}{4}) - k_y^2(Dt + \frac{w^2}{4})} \quad (\text{B2})$$

344 where  $t$  [T] is age of the couplet. Parseval's Theorem states that the integral of the squared  
 345 amplitudes of a Fourier transform equals the sum of squares of the original signal. Rough-  
 346 ness has a mean of zero, so in this case Parseval's Theorem is directly related to topo-  
 347 graphic variance and we obtain a time-evolution of topographic variance of a single pit-  
 348 mound couplet. This step yields,

$$349 \quad \sigma_{\zeta}^2(t) = \frac{1}{4\pi^2 H} \int_{-\infty}^{\infty} \int_{-\infty}^{\infty} |\hat{\zeta}(k_x, k_y, t)|^2 dk_x dk_y = \frac{A^2 w^2 l^2 \pi}{32H} \left(\frac{l^2}{4} + Dt\right)^{-3/2} \left(\frac{w^2}{4} + Dt\right)^{-1/2}, \quad (\text{B3})$$

350 where  $H$  [ $\text{L}^2$ ] is the area of the domain. The topographic variance of an entire hillslope  
 351 is the integral over all couplets of all ages which is presented in (6). Note that the pro-  
 352 duction rate,  $p$  has units ( $\text{L}^{-2} \text{T}^{-1}$ ) so that  $H$  is now included in  $p$ .

## 353 Acknowledgments

354 Data and Python scripts used to generate data are available at [https://github.com/tdoane/Topographic-](https://github.com/tdoane/Topographic-Variance/)  
 355 [Variance/](https://github.com/tdoane/Topographic-Variance/) and will be available in a maintained in the IUScholarWorks repository upon

356 publication (<https://openscholarship.indiana.edu/data-deposit>). This project was sup-  
 357 ported by the Environmental Resilience Institute, funded by Indiana University's Pre-  
 358 pared for Environmental Change Grand Challenge initiative.

## 359 References

- 360 Anderson, R. S. (2002). Modeling the tor-dotted crests, bedrock edges, and  
 361 parabolic profiles of high alpine surfaces of the Wind River Range, Wyoming.  
 362 *Geomorphology*, *46*(1-2), 35–58. doi: 10.1016/S0169-555X(02)00053-3
- 363 Booth, A. M., LaHusen, S. R., Duvall, A. R., & Montgomery, D. R. (2017).  
 364 Holocene history of deep-seated landsliding in the north fork stillaguamish  
 365 river valley from surface roughness analysis, radiocarbon dating, and numerical  
 366 landscape evolution modeling. *Journal of Geophysical Research: Earth Surface*,  
 367 *122*(2), 456–472. doi: 10.1002/2016JF003934
- 368 Brantley, S. L., Eissenstat, D. M., Marshall, J. A., Godsey, S. E., Balogh-Brunstad,  
 369 Z., Karwan, D. L., ... Weathers, K. C. (2017). Reviews and syntheses: on  
 370 the roles trees play in building and plumbing the critical zone. *Biogeosciences*,  
 371 *14*(22), 5115–5142. doi: 10.5194/bg-14-5115-2017
- 372 Brantley, S. L., McDowell, W. H., Dietrich, W. E., White, T. S., Kumar, P., An-  
 373 derson, S. P., ... Gaillardet, J. (2017). Designing a network of critical zone  
 374 observatories to explore the living skin of the terrestrial Earth. *Earth Surface*  
 375 *Dynamics*, *5*(4), 841–860. doi: 10.5194/esurf-5-841-2017
- 376 Culling, W. E. H. (1963). Soil creep and the development of hillside slopes. *The*  
 377 *Journal of Geology*, *71*(2), 127–161. (ISBN: 0022-1376 Publisher: University of  
 378 Chicago Press)
- 379 Deshpande, N., Furbish, D., Arratia, P., & Jerolmack, D. (2021). The fragility of  
 380 creeping hillslopes. *Nature Communications*, *12*(3909). doi: 10.1038/s41467-  
 381 -021-23979-z
- 382 Doane, T. H., Furbish, D. J., Roering, J. J., Schumer, R., & Morgan, D. J. (2018).  
 383 Nonlocal sediment transport on steep lateral moraines, eastern Sierra Nevada,  
 384 California, USA. *Journal of Geophysical Research: Earth Surface*, *123*(1),  
 385 187–208. doi: 10.1002/2017JF004325
- 386 Ferdowsi, B., Ortiz, C. P., & Jerolmack, D. J. (2018). Glassy dynamics of land-  
 387 scape evolution. *Proceedings of the National Academy of Sciences*, *115*(19),

- 388 4827–4832. doi: 10.1073/pnas.1715250115
- 389 Fernandes, N. F., & Dietrich, W. E. (1997). Hillslope evolution by diffusive pro-  
390 cesses: The timescale for equilibrium adjustments. *Water Resources Research*,  
391 33(6), 1307–1318. doi: 10.1029/97WR00534
- 392 Ferrier, K. L., & Kirchner, J. W. (2008, August). Effects of physical erosion  
393 on chemical denudation rates: A numerical modeling study of soil-mantled  
394 hillslopes. *Earth and Planetary Science Letters*, 272(3-4), 591–599. doi:  
395 10.1016/j.epsl.2008.05.024
- 396 Furbish, D. J., & Fagherazzi, S. (2001). Stability of creeping soil and implications  
397 for hillslope evolution. *Water Resources Research*, 37(10), 2607–2618. doi: 10  
398 .1029/2001WR000239
- 399 Furbish, D. J., & Haff, P. K. (2010). From divots to swales: Hillslope sediment  
400 transport across diverse length scales. *Journal of Geophysical Research: Earth  
401 Surface*, 115(F3). doi: 10.1029/2009JF001576
- 402 Furbish, D. J., Haff, P. K., Dietrich, W. E., & Heimsath, A. M. (2009). Statistical  
403 description of slope-dependent soil transport and the diffusion-like coefficient.  
404 *Journal of Geophysical Research*, 114, F00A05. doi: 10.1029/2009JF001267
- 405 Gabet, E. J., & Mudd, S. M. (2010). Bedrock erosion by root fracture and tree  
406 throw: A coupled biogeomorphic model to explore the humped soil production  
407 function and the persistence of hillslope soils. *Journal of Geophysical Research:  
408 Earth Surface*, 115(F4). (Publisher: Wiley Online Library)
- 409 Gabet, E. J., Reichman, O. J., & Seabloom, E. W. (2003). The effects of biotur-  
410 bation on soil processes and sediment transport. *Annual Review of Earth and  
411 Planetary Sciences*, 31(1), 249–273. doi: 10.1146/annurev.earth.31.100901  
412 .141314
- 413 Gallaway, J. M., Martin, Y. E., & Johnson, E. A. (2009). Sediment transport due to  
414 tree root throw: integrating tree population dynamics, wildfire and geomorphic  
415 response. *Earth Surface Processes and Landforms*, 34(9), 1255–1269. doi:  
416 10.1002/esp.1813
- 417 Glade, R. C., Fratkin, M. M., Pouragha, M., Seiphoori, A., & Rowland, J. C. (2021).  
418 Arctic soil patterns analogous to fluid instabilities. *Proceedings of the National  
419 Academy of Sciences*, 118(21). doi: 10.1073/pnas.2101255118
- 420 Hancock, G., & Lowry, J. (2021). Quantifying the influence of rainfall, vegetation

- 421 and animals on soil erosion and hillslope connectivity in the monsoonal tropics  
422 of northern australia. *Earth Surface Processes and Landforms*.
- 423 Heimsath, A. M., Dietrich, W. E., Nishiizumi, K., & Finkel, R. C. (2001). Stochastic  
424 processes of soil production and transport: erosion rates, topographic variation  
425 and cosmogenic nuclides in the Oregon Coast Range. *Earth Surface Processes  
426 and Landforms*, *26*(5), 531–552. doi: 10.1002/esp.209
- 427 Hellmer, M. C., Rios, B. A., Ouimet, W. B., & Sibley, T. R. (2015). Ice storms, tree  
428 throw, and hillslope sediment transport in northern hardwood forests. *Earth  
429 Surface Processes and Landforms*, *40*(7), 901–912. doi: 10.1002/esp.3690
- 430 Johnstone, S. A., & Hilley, G. E. (2015). Lithologic control on the form of soil-  
431 mantled hillslopes. *Geology*, *43*(1), 83–86. doi: 10.1130/G36052.1
- 432 Jyotsna, R., & Haff, P. K. (1997). Microtopography as an indicator of modern hill-  
433 slope diffusivity in arid terrain. *Geology*, *25*(8), 695–698. doi: 10.1130/0091-  
434 -7613(1997)025(0695:MAAIOM)2.3.CO;2
- 435 LaHusen, S. R., Duvall, A. R., Booth, A. M., & Montgomery, D. R. (2016). Sur-  
436 face roughness dating of long-runout landslides near oso, washington (usa),  
437 reveals persistent postglacial hillslope instability. *Geology*, *44*(2), 111–114. doi:  
438 10.1130/G37267.1
- 439 Lebedeva, M. I., & Brantley, S. L. (2013). Exploring geochemical controls on  
440 weathering and erosion of convex hillslopes: beyond the empirical regolith pro-  
441 duction function. *Earth Surface Processes and Landforms*, *38*(15), 1793–1807.  
442 doi: 10.1002/esp.3424
- 443 Maher, K. (2010). The dependence of chemical weathering rates on fluid residence  
444 time. *Earth and Planetary Science Letters*, *294*(1-2), 101–110. doi: 10.1016/  
445 j.epsl.2010.03.010
- 446 Martin, Y., Johnson, E., & Chaikina, O. (2013). Interplay between field obser-  
447 vations and numerical modeling to understand temporal pulsing of tree root  
448 throw processes, canadian rockies, canada. *Geomorphology*, *200*, 89–105. doi:  
449 10.1016/j.geomorph.2013.04.017
- 450 Milodowski, D. T., Mudd, S. M., & Mitchard, E. T. A. (2015). Topographic rough-  
451 ness as a signature of the emergence of bedrock in eroding landscapes. *Earth  
452 Surface Dynamics*, *3*(4), 483–499. doi: 10.5194/esurf-3-483-2015
- 453 Mudd, S. M., & Furbish, D. J. (2004). Influence of chemical denudation on hills-

- 454       lope morphology: INFLUENCE OF CHEMICAL DENUDATION ON HILL-  
455       SLOPES. *Journal of Geophysical Research: Earth Surface*, 109(F2). doi:  
456       10.1029/2003JF000087
- 457       Novick, K., & Phillips, R. (2020). *Ameriflux us-mms morgan monroe state forest*  
458       (No. 18-5). AmeriFlux AMP. doi: 10.17190/AMF/1246080
- 459       Phillips, J. D., Šamonil, P., Pawlik, I., Trochta, J., & Daněk, P. (2017). Domination  
460       of hillslope denudation by tree uprooting in an old-growth forest. *Geomorphol-*  
461       *ogy*, 276, 27–36. doi: 10.1016/j.geomorph.2016.10.006
- 462       Richardson, P. W., Perron, J. T., & Schurr, N. D. (2019). Influences of climate and  
463       life on hillslope sediment transport. *Geology*, 47(5), 423–426. (Publisher: Geo-  
464       ScienceWorld)
- 465       Riebe, C. S., Kirchner, J. W., & Finkel, R. C. (2003). Long-term rates of chemical  
466       weathering and physical erosion from cosmogenic nuclides and geochemical  
467       mass balance. *Geochimica et Cosmochimica Acta*, 67(22), 4411–4427. doi:  
468       10.1016/S0016-7037(03)00382-X
- 469       Roering, J. J., Kirchner, J. W., & Dietrich, W. E. (2001). Hillslope evolution by  
470       nonlinear, slope-dependent transport: Steady state morphology and equilib-  
471       rium adjustment timescales. *Journal of Geophysical Research: Solid Earth*,  
472       106(B8), 16499–16513. doi: 10.1029/2001JB000323
- 473       Roering, J. J., Perron, J. T., & Kirchner, J. W. (2007). Functional relationships  
474       between denudation and hillslope form and relief. *Earth and Planetary Science*  
475       *Letters*, 264(1-2), 245–258. doi: 10.1016/j.epsl.2007.09.035
- 476       Roth, D. L., Doane, T. H., Roering, J. J., Furbish, D. J., & Zettler-Mann, A.  
477       (2020). Particle motion on burned and vegetated hillslopes. *Proceed-*  
478       *ings of the National Academy of Sciences*, 117(41), 25335–25343. doi:  
479       10.1073/pnas.1922495117
- 480       Schaeztl, R. J., Burns, S. F., Small, T. W., & Johnson, D. L. (1990). Tree uprooting:  
481       Review of types and patterns of soil disturbance. *Physical Geography*, 11(3),  
482       277–291. doi: 10.1080/02723646.1990.10642407
- 483       Schaeztl, R. J., & Follmer, L. R. (1990). Longevity of treethrow microtopography:  
484       implications for mass wasting. *Geomorphology*, 3(2), 113–123. doi: 10.1016/  
485       0169-555X(90)90040-W
- 486       Struck, M., Jansen, J. D., Fujioka, T., Codilean, A. T., Fink, D., Egholm, D. L., ...

- 487 Kotevski, S. (2018). Soil production and transport on postorogenic desert  
488 hillslopes quantified with  $^{10}\text{Be}$  and  $^{26}\text{Al}$ . *GSA Bulletin*, *130*(5-6), 1017–1040.  
489 doi: 10.1130/B31767.1
- 490 Syvitski, J. P. (2003). Supply and flux of sediment along hydrological pathways: re-  
491 search for the 21st century. *Global and Planetary Change*, *39*(1-2), 1–11. doi:  
492 10.1016/S0921-8181(03)00008-0
- 493 Thompson, T., & Sowder, K. (2005). *Map showing surficial and bedrock geology of*  
494 *indiana* (No. Open-File Study 05-01).
- 495 Šamonil, P., Egli, M., Steinert, T., Norton, K., Abiven, S., Daněk, P., ...  
496 Tikhomirov, D. (2020). Soil denudation rates in an old-growth mountain  
497 temperate forest driven by tree uprooting dynamics, central europe. *Land*  
498 *Degradation & Development*, *31*(2), 222–239.
- 499 Šamonil, P., Schaetzl, R., Valtera, M., Goli, V., Baldrian, P., Vakov, I., ... Hort,  
500 L. (2013). Crossdating of disturbances by tree uprooting: Can treethrow mi-  
501 crotopography persist for 6000years? *Forest Ecology and Management*, *307*,  
502 123–135. doi: 10.1016/j.foreco.2013.06.045
- 503 Worman, S. L., & Furbish, D. J. (2019). A probabilistic, biologically informed  
504 model of desert shrub population dynamics with the granularity appropriate  
505 for geomorphic simulations. *Earth Surface Processes and Landforms*, *44*(6),  
506 1221–1232. doi: 10.1002/esp.4568
- 507 Yoo, K., Amundson, R., Heimsath, A. M., Dietrich, W. E., & Brimhall, G. H.  
508 (2007). Integration of geochemical mass balance with sediment transport to  
509 calculate rates of soil chemical weathering and transport on hillslopes. *Journal*  
510 *of Geophysical Research*, *112*(F2), F02013. doi: 10.1029/2005JF000402